ACOUSTIC MICROSCOPY OF CERAMICS*

L. W. Kessler, D. E. Yuhas and C. L. Vorres
Sonoscan Inc.
530 E. Green Street
Bensenville, Illinois

ABSTRACT

The scanning laser acoustic microscope (SLAM) is applied to the problem of nondestructive testing of ceramic materials. The employment of a very high resolution ultrasonic imaging instrument provides capabilities which supplement ultrasonic pulse-echo testing. In addition, by means of showing a picture of the flaw, the SLAM technique provides its own capabilities which alleviate some of the limitations of other techniques. Flaws of various types are documented in this paper.

INTRODUCTION

A desirable performance goal for an ultrasonic inspection method is to be able to confidently and rapidly obtain information on the presence of flaws, on their size, shape and location, and in the case of an inclusion, an identification of the foreign material. With the above information and an a priori knowledge of what constitutes a critical flaw, a decision can be made concerning accepting or rejecting the piece being inspected. With regard to characterizing small flaws (e.g. in ceramic materials) there are obstacles to meeting the above goals by means of "conventional" (pulse echo) ultrasonic testing technique.

In the "pulse-echo" technique the "signal" from the flaw depends upon many factors, for example the flaw characteristics as well as its location within a non-uniform acoustic field produced by the inspection transducer. Since the transducer integrates the acoustic signal over its entire face, a composite signal is generated which depends upon the flaw size relative to the transducer area. The flaw within the material being tested might not be a single-regular-shaped entity such as an idealized spherical inclusion (which would be amenable to mathematical analysis). In fact a typical flaw may be an irregularly shaped inclusion with pores or microcracks alongside. The sample surface might not be flat as well, thus making the scanning operation difficult in searching for flaws.

No single technique can alleviate all the above problems, however, an imaging approach can serve useful functions in these areas: (1) to provide a basis for interpreting conventional ultrasonic signals, (2) to independently provide diagnostic information on flaws, and (3) to rapidly scan large areas for suspicious structures. Though an imaging system generally requires more sophisticated equipment compared to a pulse-echo type flaw detector, often the information obtained (pictorial image) is simpler to interpret.

ACOUSTIC MICROSCOPY

With all imaging techniques the acoustic field is probed on a point-by-point basis instead of being integrated into a composite electrical signal. The scanning can be a slow raster generated by a mechanical apparatus, such as a C-scan system or by more rapid electronic scanning with full grey images. If the images are produced rapidly enough, the potential exists for an on-line quality control inspection.

The results obtained in the paper were obtained on a commercially available Scanning Laser Acoustic Microscope (SLAM) operating at 100 MHz. This instrument, by virtue of the high frequencies employed (viz 30-500 MHz) make it capable of achieving very high resolution, and which, by its novel scanning-laser-ultrasonic detection scheme make it capable of very rapid imagery (30 images per second, typical). The principal of operation of the SLAM is described in the literature and will not be discussed here.

The lower limit on detectable flaw size is set by the wavelength. The resolution, i.e. the smallest defect which can be identified in terms of lateral dimensions is on the order of 25 microns at 100 MHz, which is half an acoustic wavelength. However, the detectability, i.e. the smallest defect which can be found without focusing, is an order of magnitude better. For example, delaminations that have openings of one micron or less, have been detected as long as their spatial extent is on the order of 25 microns. In the case of microporosity, materials which have sub-resolution porosity can be differentiated on the basis of attenuation characteristics of the sample.

There are two types of acoustic micrographs (images) that will be described. The first is a normal amplitude image in which the brightness of the CRT screen relates to corresponding levels of acoustic energy within the field. The second type of image is an interferogram in which the received acoustic signal is electronically mixed with a phase reference signal so that changes in the velocity of sound propagation through various parts of the sample will be displayed on the screen. Interferograms are characterized by vertical fringes whose spacing will be uniform and straight if the velocity of sound is uniform in a flat specimen. Lateral position shifts of the fringes can be used to calculate change in material properties.

The purpose of this paper is to review the use of SLAM for NDE of ceramics. Results obtained on metals have been reported elsewhere.

*Portions of this work were supported by the ARPA/AFML program on Quantitative NDE administered through Rockwell International Science Center, Thousand Oaks, California.

Figure 1 is a disc of hot pressed silicon nitride which is shown in both modes, amplitude (top) and interferogram (bottom). The scale is 3 mm horizontally and there appears to be a fair degree of uniformity in this material. The interferogram, whose fringes are spaced by 85 micrometers, reveals slight deviations in the horizontal direction which are due to 3 micron changes in the sample thickness resulting from surface grinding. The grooves also act as acoustic scatterers which are evident as the diagonal structure on the amplitude micrograph.

In order to maximize the information obtained from an acoustic microscope there are several parameters to consider. One would like the highest resolution possible, but, unfortunately, the higher frequencies are also more highly attenuating by the material and there is less signal to noise ratio. Furthermore, as the frequency is increased (and the wavelength gets shorter) surface roughness becomes more critical; here, sample preparation can play an important role. Therefore, one has to compromise resolution, penetration and sample preparation (if it is allowable).

CHARACTERISTICS OF TYPICAL FLAWS

Several types of flaws such as delaminations, cracks, surface cracks and solid or void type inclusions in materials will be described. Figure 2 shows a ceramic chip capacitor which is an electronic component constructed of many layers of barium titanate ceramic material separated by interlayer metal electrodes. Figure 3 is a magnified optical image of a capacitor that has been destructively cross-sectioned. The thickness of each ceramic layer is approximately 25 microns and each electrode layer is about 2 1/2 microns. This image shows typical defects that are found, for example, delamination at the electrode layer and distributed porosity in the ceramic material. When an acoustic micrograph is produced of this component, the acoustic energy is directed up through the stack rather than parallel to the layers.

Figure 4 is a 30 MHz acoustic interferogram of a typical good ceramic chip capacitor whose size is approximately 6 x 9 mm. The interferogram fringes are fairly straight and uniform indicating uniform density of the ceramic. It is well established that porosity in sintered materials is associated with increased acoustic attenuation and decreased velocity of sound compared with fully dense material. If there are inhomogeneties evident within the field of view of the microscope, fringe deviations and/or dark areas would be evident. If a delamination exists, a corresponding area of reduced acoustic transmission will be evident as seen in Fig. 5. Notice that in a delamination there may still be a slight amount of transmission, but the fringes typically become somewhat scrambled indicating a loss of coherence of the wave. The bright border area, seen in Figs. 4 and 5, is where the acoustic energy is viewed directly, i.e. without passing through the sample. A comparison of the electrical signal levels can be used to ascertain the attenuation characteristics of the sample quantitatively.

Now suppose that the ceramic capacitor is soldered onto an alumina (Al_2O_3) substrate for use in a hybrid microcircuit. Prior to the soldering operation we determined that the layers were all intact and free of delamination. Now we can determine the integrity of the solder joints by observing the transmission level through the Al_2O_3-solder-capacitor structure. In Fig. 6, we observe good acoustic transmission in the areas of the bonds, i.e. at either end of the 2 x 1.5 mm capacitor, and therefore, conclude that the bonds are good.

Suppose that a sample has a surface crack. As shown in Fig. 7 acoustic energy incident upon the crack from below, will partially convert into propogating modes that travel along and parallel to the surface. The discussion here is particularly relevant to cracks that are shallow, that is, perhaps not more than a few wavelengths of sound deep; at 100 MHz, 25-100 microns would be typical. Referring to the diagram, the area to the far right of the crack at the top surface of the sample has acoustic energy from two sources, a surface mode originating from the crack and a transmitted bulk wave from the bottom. The two waves, which are coherent, will interfere and cause a characteristic cone-shaped pattern in the acoustic micrograph. Figure 8 shows an acoustic micrograph of a hot pressed silicon nitride sample which has a ground (not polished) surface and a surface crack (arrow) produced by a Vickers hardness tester instrument. The cone-shaped interference pattern is quite evident and extends well beyond the flaw site. This latter observation is useful for easily locating surface flaws since the pattern, not the crack itself, is all that need be detected. Looking at the surface in the SEM, Fig. 9, one sees the physical indentation due to the Vickers diamond stylus. Beneath the indent there is a half-penny shaped crack which cnnot be seen.

If the crack is deep as illustrated in Fig.10, and if the incident waves are at an angle with respect to the surface normal, there will be an acoustic shadow, (low transmission area) because the ultrasound will not jump across the air-filled opening. The measured width of the shadow will permit one to determine the depth of the crack provided the angle of insonification is known.

Figure 11 is an acoustic micrograph of a cracked alumina Al_2O_3 substrate a few millimeters thick. The sharp onset of the shadow defines the location of the crack at the top surface and the shadow width, about 1 mm, indicates that the crack is also 1 mm deep. (The insonification is at 45°.) The grainy structure in the image is caused by the nonuniform microstructure of the alumina itself. Full density alumina, which this is not, has a very clean acoustic transmission characteristic. The nature of the diffraction pattern will depend on the size and shape of the flaw, and also upon whether the flaw is opaque or transmissive to the acoustical wave.

If an inclusion or a void is buried deep beneath the surface of a material and viewed in the SLAM there will be scattered and transmitted energy which will interfere with each other giving rise to a diffraction pattern. This is illustrated in Fig. 12.

Figure 13 is the acoustic micrograph of a 400 micron iron inclusion implanted within a silicon nitride disc. It is located about 3 mm below the surface which is beyond the near field zone of the flaw. There is a characteristic bright diffraction ring in the center and some higher order rings surrounding it. As the flaw gets closer to the surface the image characteristic changes in a well defined manner. A series of acoustic micrographs was generated by sequentially grinding the surface thereby moving it closer towards the flaw. This sequence is shown in Fig. 14. Note that as the flaw gets closer to the image plane (the surface) the diffraction effects are reduced. These effects are an inevitable consequence of any imaging system. In order to determine the flaw size from the image we measure the image of the flaw to the first ring, then the flaw depth by stereometry. With these two data points the flaw size is determined. In the near field of the flaw we don't see diffraction rings and the flaw size is the same as its image.

To complicate life a little more, Fig. 15 indicates a common problem: flaws are not necessarily singular entities. This is a silicon inclusion located in silicon nitride and there is also some concentrated porosity (dark zones) in the same area of the sample. The SLAM image clearly differentiates the two effects. Suppose we were to try conventional high frequency ultrasonic testing. In this particular image, the horizontal field of view is 3 mm. As a side note, typical pulse-echo transducers are about this size or larger. Thus we could expect some difficulty distinguishing the two flaw types from echo signals.

In addition to flat and test samples, the SLAM can be adapted for use on complex geometries. Work has already been performed on turbine blades, tubes and other odd shaped components. In each of these cases, it is up to the investigator to select and optimize an entrance and exit port for the ultrasonic energy. Curved samples will necessarily cause corresponding curvatures to the interference fringes. For example, preliminary experiments have been performed on cylindrical ceramic test bars that are going to be subjected to tensile strength testing. The material is silicon nitride and a photograph of the sample is shown in Fig. 16. An interferogram of a good zone as compared with a suspicious zone is shown in Fig. 17 and it is evident that the differences are clearly distinguishable even though the fringes are curved.

FUTURE WORK

Our approach for further work involves 2 parallel tasks. First, analytical procedures for diffraction phenomenon which have been developed will be brought to bear on SLAM images in order to get as much quantitative information about the flaw as is possible. The second task involves establishing a data flaw library with destructive correlative analysis on naturally occurring flaws. This will guide the analysis work and can be employed to interpret flaw images on actual components which are too complicated for mathematical analysis.

BIBLIOGRAPHY

Kessler, L.W., and Yuhas, D.E., "Acoustic Microscopy 1979", Proc. IEEE, 67, (4) pp. 526-536 (1979).

Kessler, L.W., and Yuhas, D.E., "Principles & Analytical Capabilities of the Scanning Laser Acoustic Microscope", Proc. Scanning Electron Microscopy, 1978; Vol. 1, pp. 555-560, AMF O'Hare, IL. 60666.

Kupperman, D.S., et. al.;"Acoustic Microscopy Techniques for Structural Ceramics", Bulletin of the American Ceramic Society, Vol. 58, No. 8 (1980) pp. 814-841.

Yuhas, D.E. and Kessler, L.W. "Defect Characterization by Means of the Scanning Laser Acoustic Microscope (SLAM)", Proc. Scanning Electron Microscopy 1980, Vol. 1, pp. 385-391, SEM Inc., AMF O'Hare, Chicago, IL . 60666.

Yuhas, D.E. and McGraw, T.E. "Acoustic Microscopy, SEM & Optical Microscopy: Correlative Investigations in Ceramics", Proc. Scanning Electron Microscopy, 1979, 1, SEM Inc., AMF O'Hare, IL. 60666, pp. 103-110.

Kupperman, D.S., et al.: "Evaluation of Ceramic Turbine Blade with an Acoustic Microscope", Proc. First Int'l. Symp. on Ultrasonic Materials Characterization, (June 7-9, 1978, National Bureau of Standards, Gaithersburg, MD.), (In Press) ed. by H. Berger (1980).

Yuhas, D.E., and Kessler, L.W., "Scanning Laser Acoustic Microscope Applied to Failure Analysis", Proc. ATFA - 78 IEEE Inc., New York, N.Y. Catalog No. 78CH1407-6 REG 6., pp. 25-29 (1978).

Yuhas, D.E., and Kessler, L.W., "SLAM the Door on Material Failure from Internal Flaws", Industrial Research & Development, pp. 108-112, July, 1980.

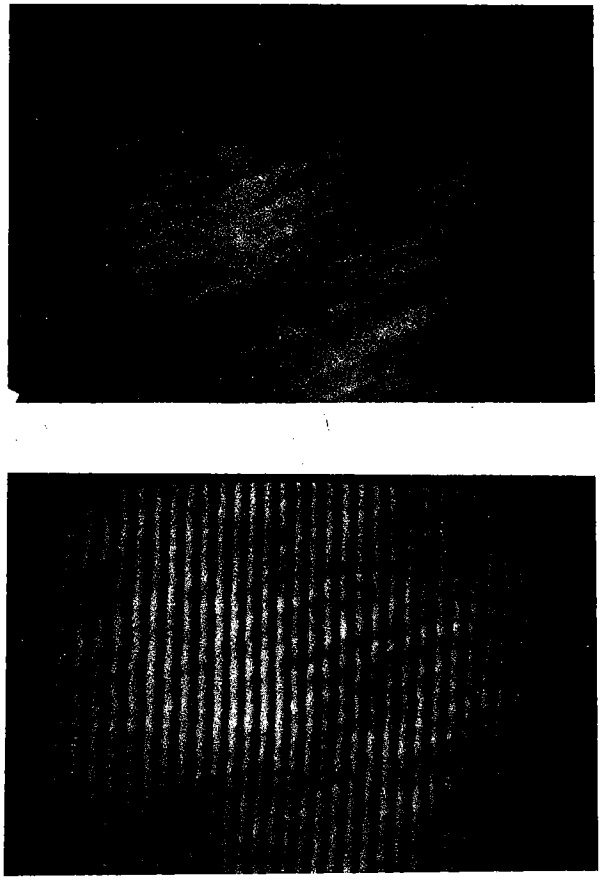

Fig. 1 - Acoustic amplitude micrograph (top) and interferogram (bottom) of a hot pressed silicon nitride disc / mm thick. The ultrasonic frequency is 100 MHz and the field of view is 3 mm horizontally.

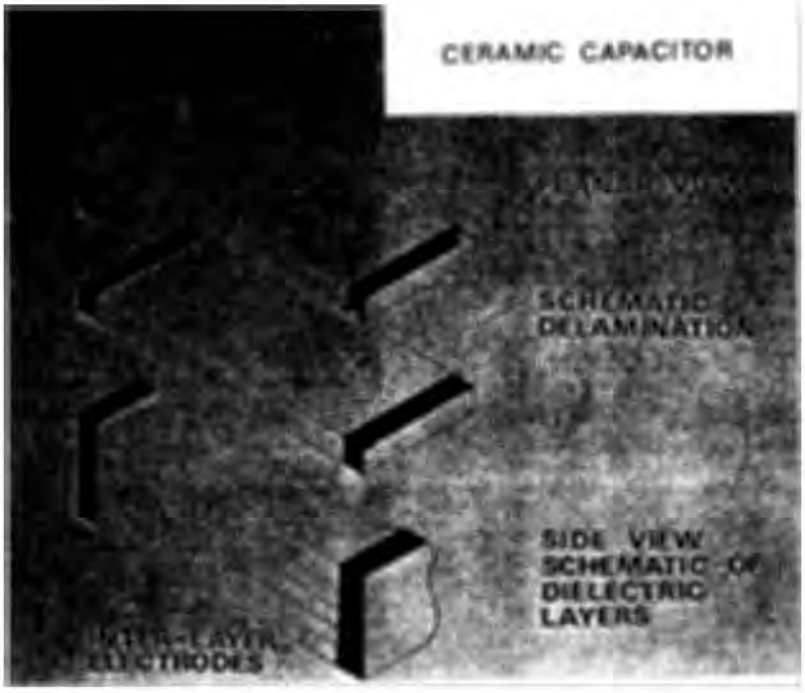

Fig. 2 - Schematic diagram of a ceramic chip capacitor consisting of multilayers of barium titanate.

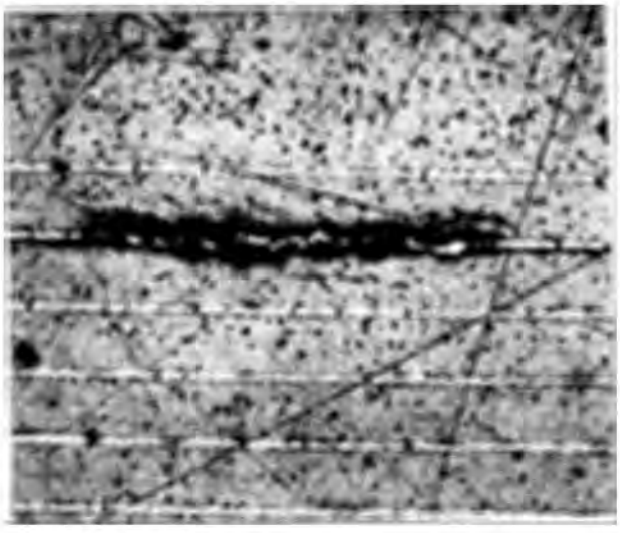

Fig. 3 - Optical view of a cross-sectioned ceramic capacitor revealing delamination at the electrode as well as porosity in the ceramic material.

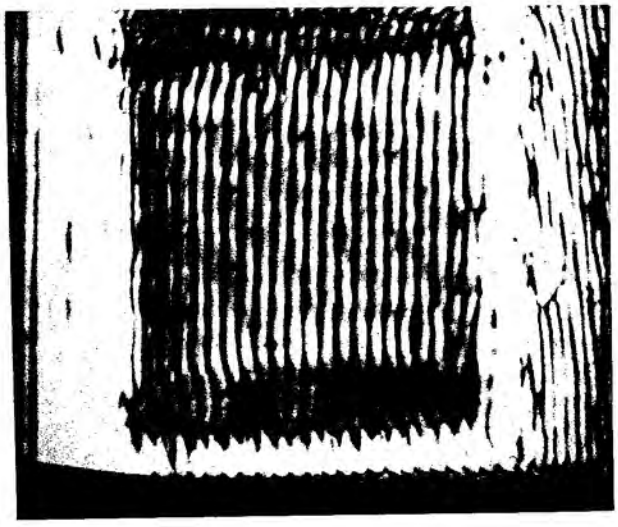

Fig. 4 - Acoustic interferogram of a typical good ceramic capacitor at an acoustic frequency of 30 MHz. The field of view is approximately 10 mm horizontally.

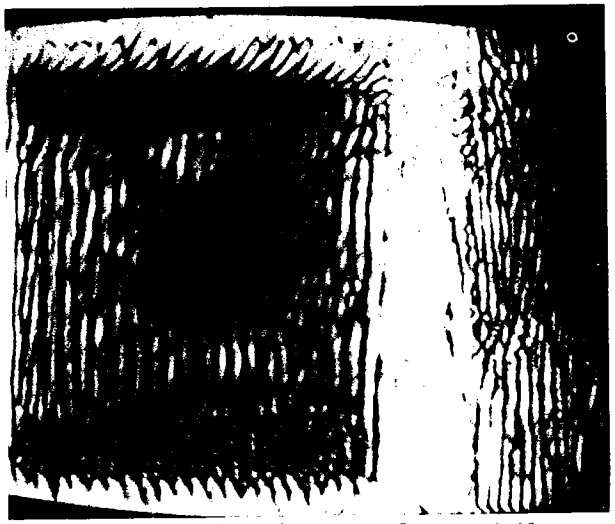

Fig. 5 - Acoustic interferogram of a partially delaminated ceramic chip capacitor.

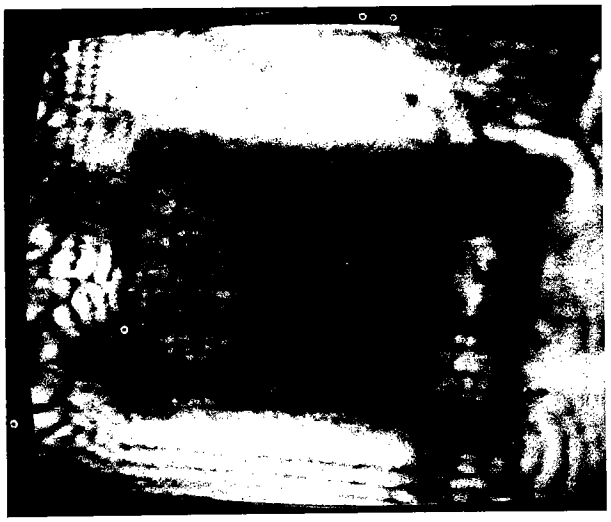

Fig. 6 - Acoustic micrograph (100 MHz) of a capacitor soldered at either end to an alumina substrate. Acoustic transmission through the ends indicates good bonding.

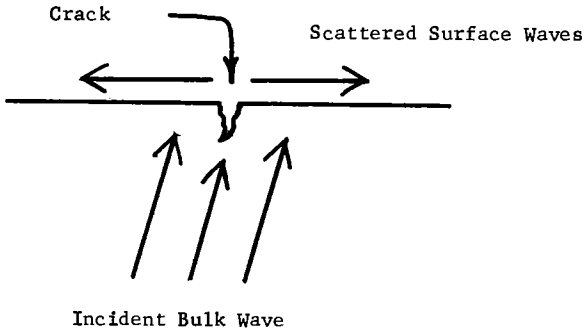

Fig. 7 - Insonification of a sample having a shallow surface crack will result in acoustic energy scattered into modes which propagate along the surface.

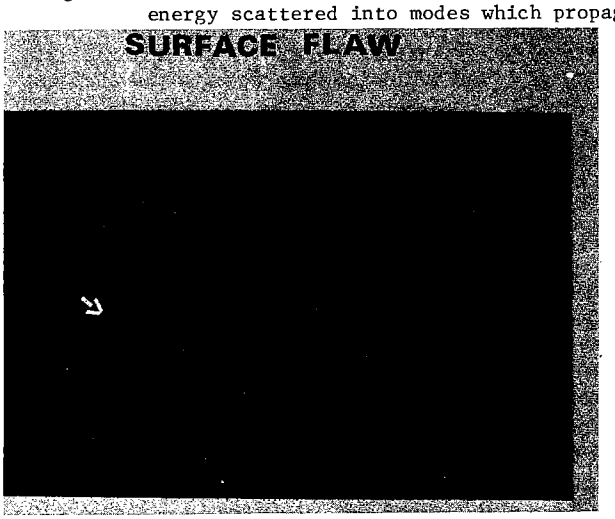

Fig. 8 - Surface flaw in hot pressed silicon nitride. The arrow indicates the site of the crack. The cone shaped interference patter extending away from the crack is caused by the mixing between the surface skimming wave travelling towards the right and the bulk wave according to Fig. 7.

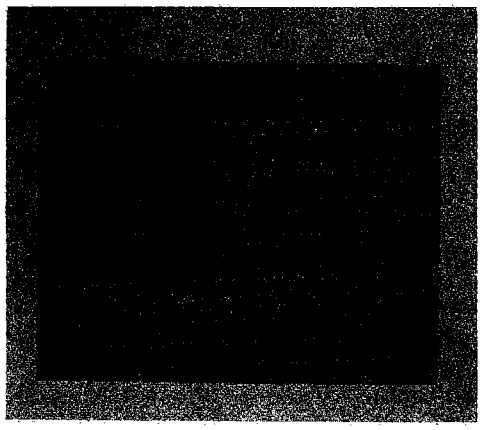

Fig. 9 - Scanning electron microscope view of Vickers indentation which caused the surface flaw on the silicon nitride sample shown in Fig. 8

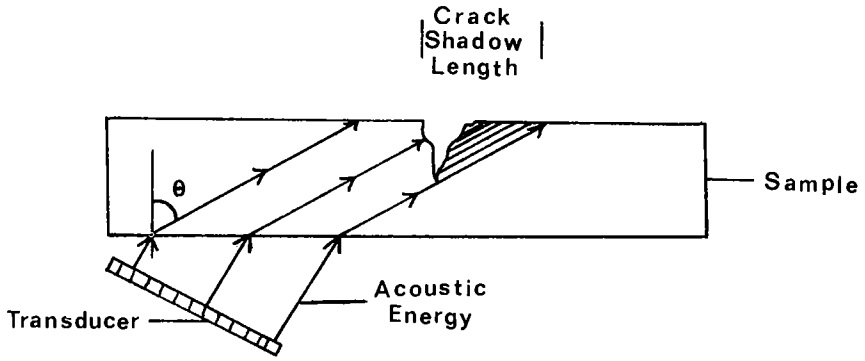

Fig. 10 - Schematic diagram illustrating insonification of a sample having a deep surface crack. A characteristic shadow is produced in the acoustic image whose dimensions are determined by the crack depth and the angle of insonification.

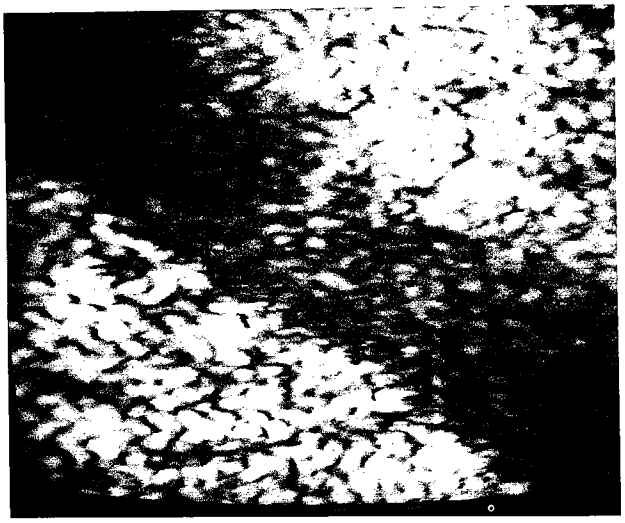

Fig. 11 - Acoustic micrograph of a 1 mm deep crack in an alumina ceramic slab.

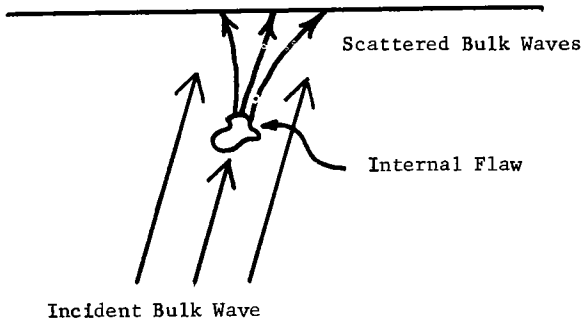

Fig. 12 - Insonification of sample having a void or inclusion deep beneath the surface.

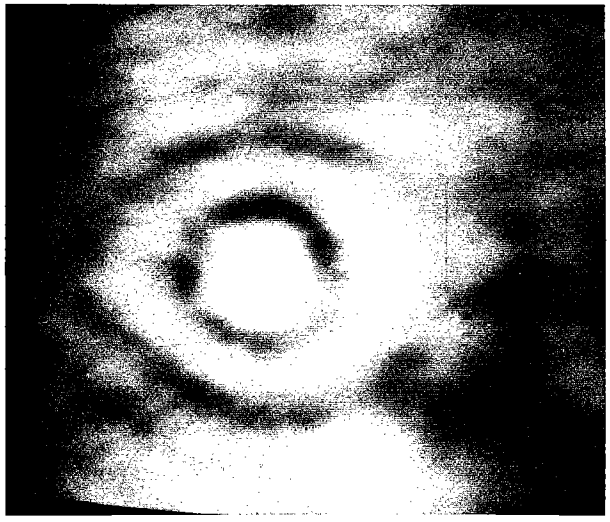

Fig. 13 - An iron inclusion, 400 microns in diameter, is located 3 mm below the surface of a hot pressed silicon nitride sample giving rise to this diffraction pattern.

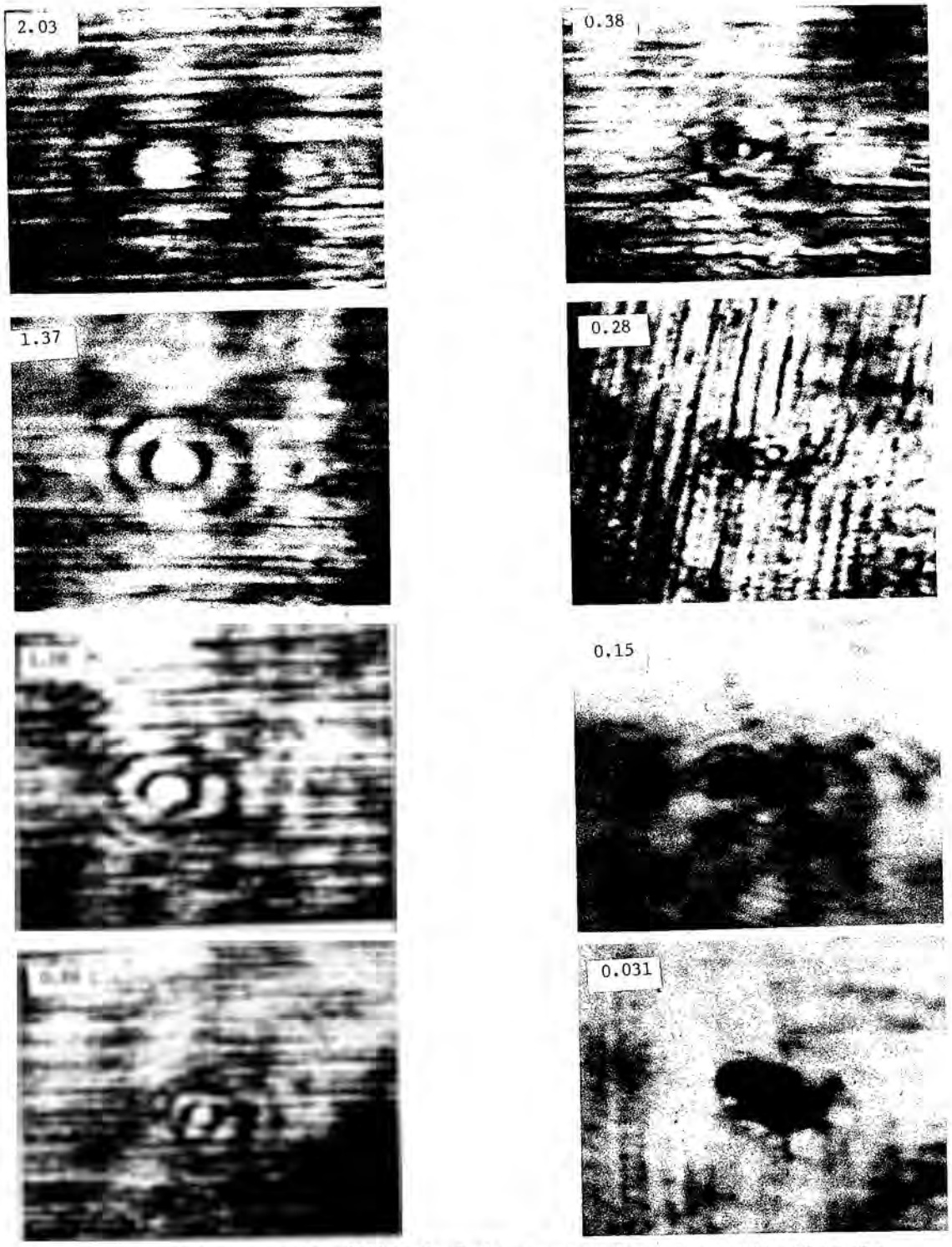

Fig. 14 - Acoustic micrographs (100 MHz) of the same iron inclusion as Fig. 12 as the thickness of the sample was reduced by grinding to bring the flaw closer to the surface. The grooves in each image are due to the rough grinding operation. The depths were measured by a simple stereoscopy technique with the acoustic microscope. The numbers in the flaw location are mi millimeters below surface.

Fig. 15 - Acoustic micrograph of a silicon inclusion and porosity with a silicon nitride sample. The porosity, which is attenuating to the acoustic wave, is located in such a position relative to the inclusion that for certain orientations of the sample one flaw masks the other.

Fig. 16 - Photograph of a cylindrical tensile bar which is made of silicon nitride.

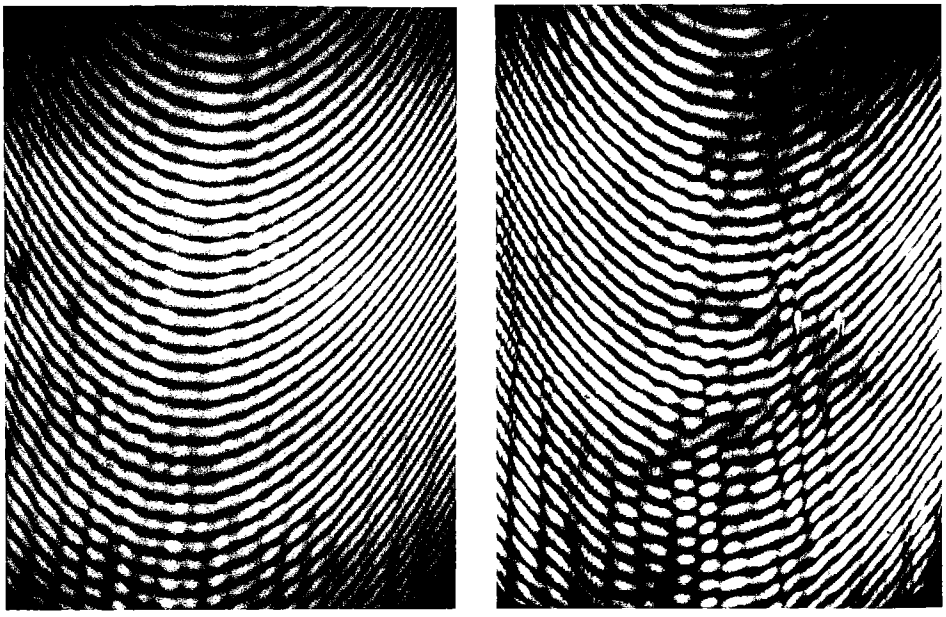

Fig. 17 - Acoustic interferograms of a typical (left) and a suspicously flawed (right) cylindrical tensile test bar shown in Fig. 16.